International Journal of Multiphase Flow 34 (2008) 879–893

Contents lists available at ScienceDirect

International Journal of Multiphase Flow

journal homepage: www.elsevier.com/locate/ijmulflow

Statistics of particle dispersion in direct numerical simulations of wall-bounded turbulence: Results of an international collaborative benchmark test

C. Marchioli [a,*], A. Soldati [a,1], J.G.M. Kuerten [b], B. Arcen [c], A. Tanière [c], G. Goldensoph [d], K.D. Squires [d], M.F. Cargnelutti [e], L.M. Portela [e]

[a] Department of Energy Technology and Centro Interdipartimentale di Fluidodinamica e Idraulica, University of Udine, Udine, Italy
[b] Department of Mechanical Engineering, Technische Universiteit Eindhoven, Eindhoven, Netherlands
[c] LEMTA, Nancy University, CNRS, ESSTIN, Vandoeuvre-lés-Nancy, France
[d] Department of Mechanical and Aerospace Engineering, Arizona State University, Tempe, USA
[e] Department of Multi-Scale Physics, Technische Universiteit Delft, Delft, Netherlands

ARTICLE INFO

Article history:
Received 17 July 2007
Received in revised form 10 January 2008
Available online 10 March 2008

Keywords:
Collaborative test case
Two-phase gas–solid flow
Direct numerical simulation
Lagrangian particle tracking
Steady-state concentration database

ABSTRACT

In this paper the results of an international collaborative test case relative to the production of a direct numerical simulation and Lagrangian particle tracking database for turbulent particle dispersion in channel flow at low Reynolds number are presented. The objective of this test case is to establish a homogeneous source of data relevant to the general problem of particle dispersion in wall-bounded turbulence. Different numerical approaches and computational codes have been used to simulate the particle-laden flow and calculations have been carried on long enough to achieve a statistically steady condition for particle distribution. In such stationary regime, a comprehensive database including both post-processed statistics and raw data for the fluid and for the particles has been obtained. The complete datasets can be downloaded from the web at HTTP://CFD.CINECA.IT/CFD/REPOSITORY/. In this paper the most relevant velocity statistics (for both phases) and particle distribution statistics are discussed and benchmarked by direct comparison between the different numerical predictions.

1. Introduction

Turbulent particle dispersion in wall-bounded flows is a fundamental issue in a number of industrial and environmental applications. Direct numerical simulation (DNS) and Lagrangian particle tracking (LPT) may be a useful tool to provide physical insights, new modeling ideas and benchmark cases (Moin and Mahesh, 2002; Yeung, 2002). Despite the large number of published works, however, it is extremely difficult to gather a uniform and complete source of data that can be used to perform a phenomenological study of some, still not well-established features of particle transport in turbulent flows or to assess the effectiveness of computer simulation models on the accuracy of predicted particle deposition rates (Sergeev et al., 2002; Tian and Ahmadi, 2007).

Lack of uniformity and of completeness in the available numerical data is connected to several reasons (associated with the intrinsic complexity of turbulent transfer phenomena) and is accompanied to uncertainty in methodologies, mostly due to the large number of physical and computational parameters involved and to the unclear influence of several of them. The main physical parameters that will influence the simulation results are the particle Stokes number, which quantifies the response of the dispersed phase to the perturbations produced by the underlying turbulence, and the flow Reynolds number. Other important parameters are related to modeling of fluid–particle interaction (one-way/two-way coupling); particle–particle interaction (collision models); particle–wall interaction (reflecting or absorbing wall, wall effects); particle rotation and modeling of forces acting on particles (e.g., the lift force). On the computational side, the treatment of discrete particles in DNS fields poses open or partly open questions on the assessment of the performance of flow solvers that use different numerical methods and on the accuracy of the interpolation scheme used to obtain the fluid velocity at the instantaneous particle location. In this context, the proper choice of parameters such as the grid resolution and the time-step size required for advancement of the governing balance equations becomes extremely important.

This paper is the result of the first necessary step towards a rigorous, systematic analysis of these issues. Specifically, the objectives of this analysis are to have a large number of people working independently on the same test case problem (DNS of particle dispersion in turbulent channel flow) and to establish a large validated database including (i) reliable and accurate velocity

* Corresponding author. Tel.: +39 0432 558006.
E-mail address: marchioli@uniud.it (C. Marchioli).
[1] Currently at EPFL, Lausanne (CH).

0301-9322/$ - see front matter © 2008 Elsevier Ltd. All rights reserved.
doi:10.1016/j.ijmultiphaseflow.2008.01.009

statistics for the fluid, for the particles and for the fluid at the particle position (mean and rms velocities, skewness and flatness, Reynolds stresses and quadrant analysis); (ii) particle concentration profiles and deposition rates; (iii) one-particle statistics (particle velocity auto-correlations, particle turbulent diffusivity, particle mean-square displacements, Lagrangian integral time scales); (iv) two-particle statistics (rms particle dispersion). Datasets come from five independent simulations and include not only the post-processed statistics just listed but also the corresponding raw data providing the evolution of the fluid velocity field and the time behavior of the particle position and velocity components: these data are made available to users who need to compute specific statistics other than those included in the database. Besides providing a homogeneous source of data on DNS and LPT not previously available, the database can be used as benchmark either to compare directly different numerical approaches or to validate engineering models for particle dispersion (e.g., two-fluid Eulerian models). The need for this type of data could be extended also to commercial softwares for computational fluid dynamics: these softwares, even though usually exploited for high-Reynolds-number flows in complex geometries, fail predictions of multiphase flows due to the lack of appropriate physical models for particle dispersion, resuspension and deposition.

The test case was conceived in 2004 at the IUTAM Symposium on Computational Approaches to Multiphase Flow (Balachandar and Prosperetti, 2006) and it was first advertised in 2005 at the 11th Workshop on Two-phase flow predictions (Sommerfeld, 2005). During the workshop, common base guidelines for participant groups were provided. The following groups (listed in random order) joined the test case calculations: (1) C. Marchioli and A. Soldati (Group UUD hereinafter), (2) J.G.M. Kuerten (Group TUE hereinafter), (3) B. Arcen and A. Tanière (Group HPU hereinafter), (4) G. Goldensoph and K. Squires (Group ASU hereinafter), (5) M.F. Cargnelutti and L.M. Portela (Group TUD hereinafter). As starting point of the test case, a DNS of dilute particle-laden turbulent channel flow at low Reynolds number has been performed by all groups following the base guidelines. Aim of this benchmark calculation is to build a thorough statistical framework including both statistically developing and statistically steady conditions for the distribution of the dispersed phase. To quantify the collaborative effort required by the test case, it should be noted that the simulation time taken for each group to achieve a statistically steady condition for the particle distribution was of the order of eight to ten months, mostly depending on the availability of computational resources. This is equivalent to an overall simulation time of about four years on standard production machines.

The present paper is organized as follows: first the physical problem and the numerical methodology adopted by each group are briefly outlined, then the performance of the different numerical approaches is benchmarked through direct comparison of the most relevant statistics for both phases. In the final section, conclusions and implications for future developments of the test case are drawn.

2. Physical problem and numerical methodology

2.1. Particle-laden turbulent channel flow

The flow into which particles are introduced is a turbulent channel flow of gas. In the present study, we consider air (assumed to be incompressible and Newtonian) with density $\rho = 1.3\ \mathrm{kg\ m^{-3}}$ and kinematic viscosity $\nu = 15.7 \times 10^{-6}\ \mathrm{m^2\ s^{-1}}$. The governing balance equations for the fluid (in dimensionless form) read as:

$$\frac{\partial u_i}{\partial x_i} = 0, \tag{1}$$

$$\frac{\partial u_i}{\partial t} = -u_j \frac{\partial u_i}{\partial x_j} + \frac{1}{Re}\frac{\partial^2 u_i}{\partial x_j^2} - \frac{\partial p}{\partial x_i} + \delta_{1,i}, \tag{2}$$

where u_i is the ith component of the dimensionless velocity vector, p is the fluctuating kinematic pressure, $\delta_{1,i}$ is the mean dimensionless pressure gradient that drives the flow and $Re_\tau = u_\tau h/\nu$ is the shear Reynolds number based on the shear (or friction) velocity, u_τ, and on the half channel height, h. The shear velocity is defined as $u_\tau = (\tau_w/\rho)^{1/2}$, where τ_w is the mean shear stress at the wall. In this benchmark calculation, the shear Reynolds number is $Re_\tau = 150$; the corresponding bulk Reynolds number is $Re_b = u_b h/\nu = 2100$ based on the bulk velocity $u_b = 1.65\ \mathrm{m\ s^{-1}}$. All variables considered in this study are reported in dimensionless form, represented by the superscript +[2] and expressed in wall units. Wall units are obtained combining u_τ, ν and ρ.

The reference geometry consists of two infinite flat parallel walls: the origin of the coordinate system is located at the center of the channel and the $x-$, $y-$ and $z-$ axes point in the streamwise, spanwise and wall-normal directions, respectively (see Fig. 1). Periodic boundary conditions are imposed on the fluid velocity field in x and y, no-slip boundary conditions are imposed at the walls. The calculations were performed on a computational domain of size $4\pi h \times 2\pi h \times 2h$, corresponding to $1885 \times 942 \times 300$ wall units in x, y and z, respectively. For ease of reading, details on the Eulerian grid used to discretize the flow domain and on the time-step size, Δt^+, employed by each group are given in Section 2.2. Here, we just mention that the base simulation requirements prescribe a minimum number of grid points in each direction to ensure that the grid spacing is always smaller than the smallest flow scale[3] and that the limitations imposed by the point-particle approach are satisfied.

Particles with density $\rho_p = 1000\ \mathrm{kg\ m^{-3}}$ are injected into the flow at concentration low enough to consider dilute system conditions (particle–particle interactions are neglected). Furthermore, particles are assumed to be pointwise, rigid and spherical. The motion of particles is described by a set of ordinary differential equations for particle velocity and position at each time step. For particles much heavier than the fluid ($\rho_p/\rho \gg 1$) Elghobashi and Truesdell (1992) have shown that the only significant forces are Stokes drag and buoyancy and that Basset force can be neglected being an order of magnitude smaller. In the base simulation, the aim is to minimize the number of degrees of freedom by keeping the simulation setting as simplified as possible; thus the effect of gravity has also been neglected. With the above assumptions the following Lagrangian equation for the particle velocity is obtained:

$$\frac{\mathrm{d}\mathbf{u}_p}{\mathrm{d}t} = -\frac{3}{4}\frac{C_D}{d_p}\left(\frac{\rho}{\rho_p}\right)|\mathbf{u}_p - \mathbf{u}|(\mathbf{u}_p - \mathbf{u}), \tag{3}$$

where $\mathbf{u}_p$ and $\mathbf{u}$ are the particle and fluid velocity vectors, d_p is the particle diameter and C_D is the drag coefficient given by Rowe and Enwood (1962):

$$C_D = \frac{24}{Re_p}(1 + 0.15 Re_p^{0.687}), \tag{4}$$

where Re_p is the particle Reynolds number ($Re_p = d_p|\mathbf{u}_p - \mathbf{u}|/\nu$). The correction for C_D is necessary because Re_p does not necessarily remain small, in particular for depositing particles.

For the simulations presented here, three particle sets were considered, characterized by different relaxation times, defined

[2] The superscript + has been dropped from Eqs. (1) and (2) for ease of reading.

[3] In the present flow configuration, the non-dimensional Kolmogorov length scale, η_K^+, varies along the wall-normal direction from a minimum value $\eta_K^+ = 1.6$ at the wall to a maximum value $\eta_K^+ = 3.6$ at the centerline. In terms of time scales, the Kolmogorov time scale, τ_K^+, varies along the wall-normal direction from a minimum value $\tau_K^+ = 2$ at the wall to a maximum value $\tau_K^+ = 13$ at the centerline (Marchioli et al., 2006).

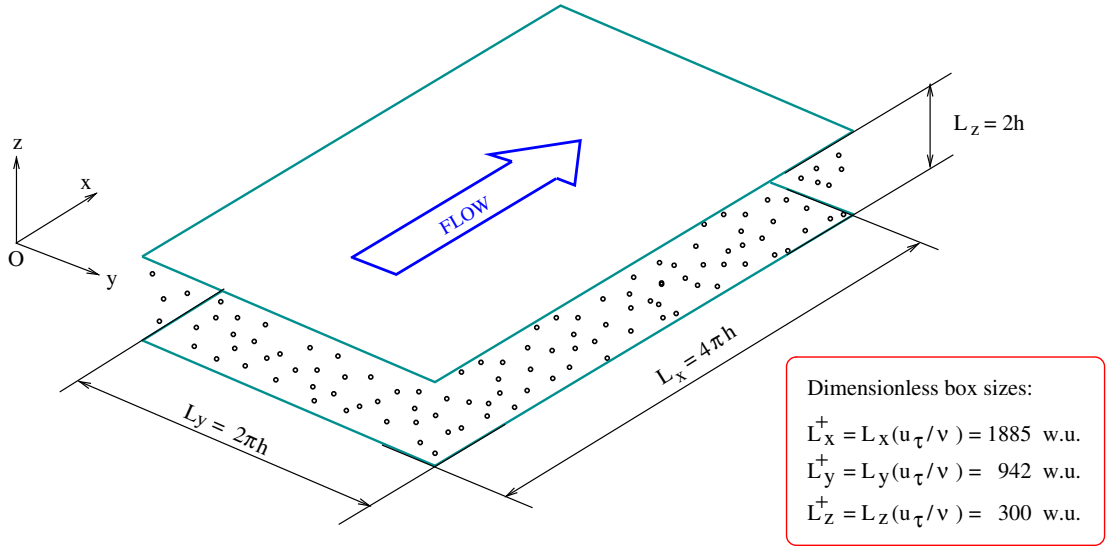

Fig. 1. Particle-laden turbulent gas flow in a flat channel: computational domain.

as $\tau_p = \rho_p d_p^2/18\mu$, where μ is the fluid dynamic viscosity. The particle relaxation time is made dimensionless using wall variables and the Stokes number for each particle set is obtained as $St = \tau_p^+ = \tau_p/\tau_f$ where $\tau_f = \nu/u_\tau^2$ is the characteristic time scale of the flow. Table 1 shows all the parameters of the particles injected into the flow field. To build the database, the "one-way coupling" approximation (under which particles do not feedback on the flow field) was considered. At the beginning of the Lagrangian tracking, particles were distributed randomly over the computational domain and their initial velocity was set equal to that of the fluid at the particle initial position. We remark here that the process of particle dispersion will not be sensitive to this initial condition if the long-term features of the motion are investigated. Regarding the boundary conditions of the dispersed phase, perfectly elastic collisions at the smooth wall were assumed when the particle center was at a distance from the wall lower than one particle radius. Further, particles moving outside of the computational domain in the streamwise and/or spanwise directions were reintroduced via periodicity.

Further details on the Lagrangian tracking (e.g., the numerosity of particle sets, the fluid velocity interpolation scheme, etc.) are given for each group in Section 2.2.

Table 1
Particle parameters

$St = \tau_p^+$	$\tau_p(s)$	d_p^+	d_p (μm)	$V_s^+ = g^+ St$	$Re_p^+ = \frac{V_s^+ d_p^+}{\nu^+}$
1	1.133×10^{-3}	0.153	20.4	0.094	0.01444
5	5.660×10^{-3}	0.342	45.6	0.472	0.16127
25	2.832×10^{-2}	0.765	102	2.360	1.80505

2.2. DNS methodology and computational resources

In this Section, the different numerical approaches and computational codes are briefly outlined. They are also summarized in Table 2, where the *numerical* degrees of freedom characterizing the benchmark calculation are presented. The possibility of using different numerical schemes and/or different values for some simulation parameters (like the time integration step size or the number of grid points, for instance) allows clearcut evaluation of how the accuracy of the DNS results depends on the choice made.

- *Group UUD:* The computational flow solver is based on the Fourier–Galerkin method in the streamwise and spanwise directions, whereas a Chebyshev-collocation method in the wall-normal direction. Time integration of fluid uses a second-order Adams–Bashforth scheme for the non-linear terms (which are calculated in a pseudo-spectral way with de-aliasing in the periodic directions) and an implicit Crank–Nicolson scheme for the viscous terms. A LPT code coupled with the DNS code is used to calculate particles paths in the flow field. The particle equation of motion is solved using a fourth-order Runge–Kutta scheme for time integration. Fluid velocities at particle position are obtained using sixth-order Lagrangian polynomials: near the wall, the interpolation scheme switches to one-sided. The total number of particles tracked is 100,000. The computational time-step size in wall units is $\Delta t^+ = 0.045$ for the fluid and $\Delta t^+ = 0.45$ for the particles, this latter value being larger than those adopted by the other groups (see Table 2). Simulations were performed running a serial version of the code on a standard production machine with Pentium IV 2.6 GHz CPU and

Table 2
Summary of numerical methodologies

Group	Flow solver	Time integration of fluid (non-linear + viscous terms)	Time integration of particles	Fluid velocity interpolation	Grid resolution ($N_x \times N_y \times N_z$)	Wall-normal distribution of collocation points
UUD	PS	AB2 + CN	RK4 ($\Delta t^+ = 0.45$)	L6	$128 \times 128 \times 129$	Chebyschev
TUE	PS	RK3 + CN	H2 ($\Delta t^+ = 0.032$)	LH4	$128 \times 128 \times 129$	Chebyschev
HPU	FD2	RK3 + CN	RK3 ($\Delta t^+ = 0.05$)	H3	$192 \times 160 \times 128$	HT (SF = 1.4)
ASU	FD2	AB2 + CN	AB2 ($\Delta t^+ = 0.05$)	H3	$128 \times 128 \times 129$	HT (SF = 1.7)
TUD	FV2	AB2	RK2 ($\Delta t^+ = 0.026$)	TL	$192 \times 192 \times 192$	HT (SF = 1.7)

Nomenclature used in this table is as follows: (i) *Flow Solver* – PS: pseudo-spectral, FD2: second-order finite differences, FV2: second-order finite volumes; (ii) *Time integration* – AB2: second-order Adams–Bashforth, CN: implicit Crank–Nicolson, RK2: second-order Runge–Kutta, RK3: third-order Runge–Kutta, RK4: fourth-order Runge–Kutta, H2: second-order Heun method, Δt^+: non-dimensional time-step size; (iii) *Fluid velocity interpolation* – L6: sixth-order Lagrange polynomials, LH4: fourth-order Lagrange–Hermite polynomials, H3: third-order Hermite polynomials. TL: Tri-linear; (iv) *Wall-normal collocation points* – HT: hyperbolic tangent (SF, stretching factor).

1 GB RAM. Further details about the numerical methodology of this group can be found in Marchioli and Soldati (2002).

- *Group TUE:* The computational flow solver is based on the Fourier–Galerkin method in the streamwise and spanwise directions, whereas a Chebyshev-collocation method is used in the wall-normal direction. Non-linear terms are calculated in a pseudo-spectral way with de-aliasing in the periodic directions. The solution is completely divergence-free through the use of the influence matrix method with full correction to remove Chebyshev-truncation errors. Time integration is performed with a third-order three-stage Runge–Kutta method for the non-linear terms and the implicit Crank–Nicolson method for the linear terms. The particle equation of motion is solved with the second-order Heun method. Fluid velocity at particle position is obtained by fourth-order accurate interpolation: Lagrange polynomials are used in the periodic directions, whereas Hermite polynomials are used in the wall-normal direction. The total number of particles tracked is 10^5. The computational time step in wall units is $\Delta t^+ = 0.032$ for both phases. Simulations were performed running a mpi-parallelized version of the code on a Linux PC cluster with 8 CPU and 8 GB RAM. Further details about the numerical methodology of this group can be found in Kuerten (2006).
- *Group HPU:* A second-order finite-difference DNS solver, based on the model proposed by Orlandi (2000), was used for the flow: time discretization is semi-implicit, i.e., the non-linear terms are written explicitly with a third-order Runge–Kutta scheme and the viscous terms are written implicitly using a Crank–Nicolson scheme. Computations were run with imposed flow rate corresponding to a bulk Reynolds number $Re_b = 2280$ based on the bulk velocity and the channel half-width. The shear Reynolds number obtained at steady state is $Re_\tau = 155$, slightly higher than that simulated by the other groups. To initialize position and velocity of the particle phase, the flow domain was divided into 128 slices along the wall-normal direction, the thickness of each slice being equal to the wall-normal grid spacing. Samples of 5000 solid particles were distributed homogeneously within each slice. The total number of particles tracked is thus 640,000. The computational time-step in wall units is $t^+ = 0.05$ for both phases. Simulations were performed running a serial version of the code on a standard production machine with Pentium IV 3.4 GHz CPU and 3 GB RAM. Further details about the numerical methodology of this group can be found in Arcen et al. (2006).
- *Group ASU:* A fractional-step method is used to solve for the NS equations. Spatial derivatives are evaluated using second-order centered differences. Time integration of fluid is performed using a second-order Adams–Bashforth scheme for the non-linear terms and an implicit Crank–Nicolson scheme for the viscous terms. A second-order Adams–Bashforth scheme is also used for time integration of particle equation of motion, and third-order Lagrange polynomials are used for fluid velocity interpolation. The total number of particles tracked is 10^5. The computational time-step in wall units is $t^+ = 0.05$ for both phases. Simulations were performed running a serial version of the code on a Pentium IV 2.6 GHz CPU and 1 GB RAM. Further details about the numerical methodology of this group can be found in Goldensoph (2006).
- *Group TUD:* A standard finite-volume code based on a predictor–corrector solver is used to solve for the NS equations on a staggered grid. Time integration of fluid is performed using a second-order Adams–Bashforth scheme. A second-order Runge–Kutta scheme is also used for time integration of particle equation of motion, and tri-linear interpolation is used to calculate the fluid velocity at the particle position. The total number of particles tracked is around 950,000. The computational time-step for the fluid is roughly $t^+ = 0.026$ in wall units, the exact size being determined adaptively. The time-step size for the particles is always equal to or smaller than the fluid time-step since it is chosen such that a particle cannot travel more that half grid cell per iteration. Simulations were performed running a serial version of the code, partially on a standard production machine with AMD Athlon 2133 MHz dual processor CPU and 2 GB RAM, and partially on one node of a SGI Altix 3700 system consisting of 416 CPUs (Intel Itanium 2, 1.3 GHz each) and 832 GB total RAM. Further details about the numerical methodology of this group can be found in Portela and Oliemans (2003).

3. Results

In this Section, some of the most relevant statistics for the fluid phase and for the particle phase are presented and discussed *vis-à-vis* to benchmark the performance of the different numerical approaches. It is important to remind the reader that all particle statistics shown in this paper refer to a steady state for particle distribution. Particle statistics were computed summing the desired variable (velocity, velocity fluctuation, etc.) over all particles in a certain sampling volume, constituted by wall-parallel fluid slab obtained as described in Section 3.2, and averaging by the number of particles in the sampling volume. This type of density-weighted statistics is particularly useful for model developers.

For sake of brevity, we will limit our analysis to the first- and second-order moments of both phases (namely the mean streamwise velocity and the rms values of the three velocity components), to the Reynolds stresses and to the particle concentration profiles. Higher-order statistics as well as two-particle statistics will not be presented here since they would not add to the discussion. The reader is referred to the raw data repository for further statistical exploration.

3.1. Fluid statistics

Fig. 2 shows the mean streamwise fluid velocity profiles, U_x^+. The profile of each group is represented using symbols, whereas the black line represents the analytical mean velocity profile given by the law of the wall, $U_x^+ = z^+$, and by the log law, $U_x^+ = 2.5 \log z^+ + 5.5$. It is apparent that the profiles almost overlap, yet a close-up view has been included in the diagram to appreciate better the behavior of U_x^+ in the outer layer of the channel, where a slight velocity deficit is observed for the profile of Group HPU. This may be due to the smaller number of grid points taken to discretize the domain along the wall-normal direction ($N_z = 128$) compared to those taken by Group TUD ($N_z = 192$) using the same second-order accurate flow solver.

Fig. 3a–c shows the root mean square (rms) of the fluid velocity ($U'_{i,rms}$) in the streamwise ($i = x$), spanwise ($i = y$) and wall-normal ($i = z$) direction, respectively. Symbols are as in Fig. 2. Results are in rather good agreement for the $U'_{x,rms}$ component (as also apparent from the close-up view in Fig. 3a) but small differences in the quantitative numbers arise for $U'_{y,rms}$ and $U'_{z,rms}$, particularly outside the buffer layer close to the channel centerline. Differences observed in the first and second-order moments of the fluctuating fluid velocity field are, of course, due solely to the specific numerical method employed by each flow solver and to the accuracy of grid discretization. These differences in modeling the flow field will add to differences in modeling the particle motion and will show up also in the statistical moments for the particle velocity.

To conclude the section devoted to fluid statistics, the results obtained for the Reynolds stresses are discussed since they may be of interest in the context of deriving models for fully developed, dilute particulate turbulent flow with a suitably closed system of

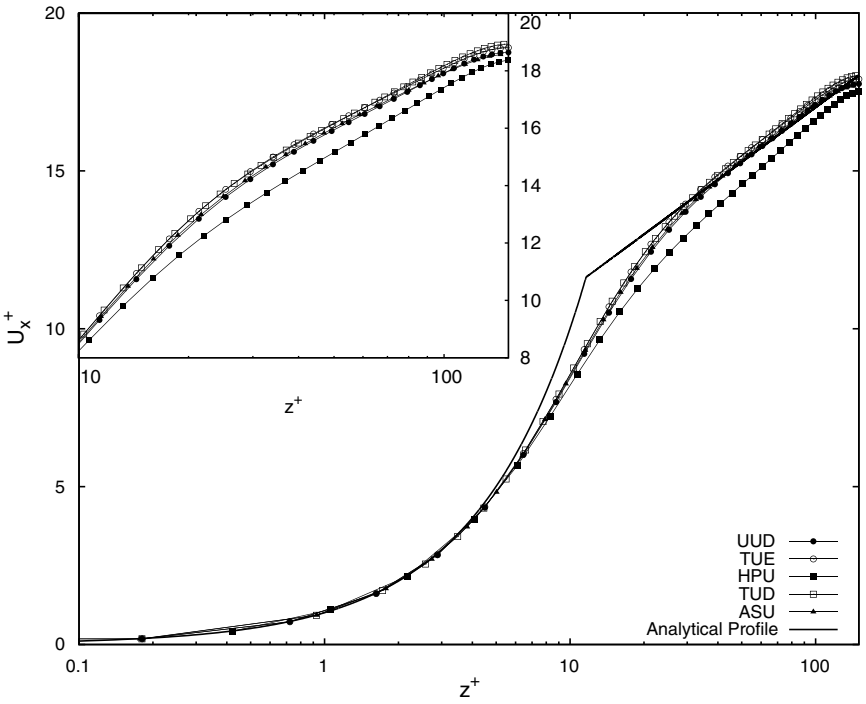

Fig. 2. Mean streamwise fluid velocity.

governing equations (Sergeev et al., 2002). Specifically, Fig. 4 shows the time- and space-averaged $(U_x^+)'(U_z^+)'$-component of the Reynolds stress tensor, $(U_x^+)'$ and $(U_z^+)'$ being the non-dimensional fluid velocity fluctuations in the streamwise direction and in the wall-normal direction, respectively. The agreement between the different profiles is indeed satisfactory, particularly if one considers that the profile of Group HPU, which does not overlap perfectly around the negative peak value and near the centerline, was obtained for a slightly higher value of the shear Reynolds number.

3.2. Particle statistics

When computing particle statistics, it is of particular importance to define precisely the computational procedure to ensure reproducibility of the results. In this study, particle statistics were computed by averaging over $N_s = 193$ wall-parallel fluid slabs distributed non-uniformly along the wall-normal direction. The thickness of the sth slab, $\Delta z^+(s)$, was obtained by means of hyperbolic-tangent binning with stretching factor $\gamma = 1.7$:

$$\Delta z^+(s) = \frac{Re_\tau}{\tanh(\gamma)}\left[\tanh\left(\gamma\frac{s}{N_s}\right) - \tanh\left(\gamma\frac{s-1}{N_s}\right)\right]. \quad (5)$$

The smallest thickness is at the wall ($\Delta z^+_{\min} = 0.361$) whereas the largest thickness is at the channel centerline ($\Delta z^+_{\max} = 2.84$). Despite the large particle concentration gradients expected near the walls, $\Delta z^+_{\min}$ was chosen slightly larger than the wall-normal grid spacing of the numerical simulation, the minimum thickness allowed at the wall being limited by the $St = 25$ particle radius (see Table 1). A particle belongs to a slab if its center is located inside the slab.

Since the aim of the benchmark simulation is to reach a statistically steady-state for the particle distribution, the process of accumulation was followed over time starting from an initial condition of randomly distributed particles. Fig. 5 shows the time evolution of the maximum value of particle number density near the wall, $n_p^{\max}$, for each particle set as obtained by the Group UUD (profiles obtained by the other groups are not shown as they provide qualitatively similar results and would not add to the discussion) up to $t^+ = 21{,}150$. The rationale for monitoring this quantity lies in the fact that the concentration close to the wall is the one that takes longer to reach its steady state. After an initial large change covering a time span of about 1000 wall time units and a slow asymptotic convergence towards a *mean* value (represented by the horizontal dashed lines in Fig. 5), this state appears to be achieved at $t^+ \simeq 20{,}000$. Since the non-dimensional bulk velocity in the channel is roughly equal to $U_x^+ = 15$, this time threshold corresponds to a *developing-length* of roughly 1000 channel heights. This number shows the difficulties, both numerical and experimental, of obtaining information on fully developed particle-laden channel flows: the *particle developing-length* can be much larger than the hydrodynamic developing-length, requiring extremely long computational times in numerical simulations, and extremely long channels (or pipes) in physical experiments.

Fig. 6 shows the particle concentration profiles, C/C_0, as function of the wall-normal coordinate, z^+, at the threshold $t^+ = 20{,}000$ and for each particle set. Concentration statistics at earlier stages of the simulations, in which a statistically developing condition for the particle concentration exists, have also been computed: datasets have been gathered past the initial transient of 1000 wall time units, taken to obtain results that are independent of the initial conditions imposed on the particles, up to the end of the simulations with saving frequency of 1000 wall time units.

Particle concentration was obtained as follows: first, the flow domain is divided into slabs according to the above-mentioned binning procedure; second, at each time-step the number of particles within each slab is determined and divided by the volume of that slab to obtain the local concentration $C = C(s)$; finally, C is normalized by its initial value, C_0. According to this procedure, the ratio C/C_0 is in fact a particle number density distribution and will be larger than unity in the flow regions were particles tend to preferentially distribute and smaller than unity in the regions depleted of particles.

From Fig. 6 we observe that, starting from an initial distribution corresponding to a flat profile centered around $C/C_0 \simeq 1$, the expected near-wall concentration build up occurs and that the

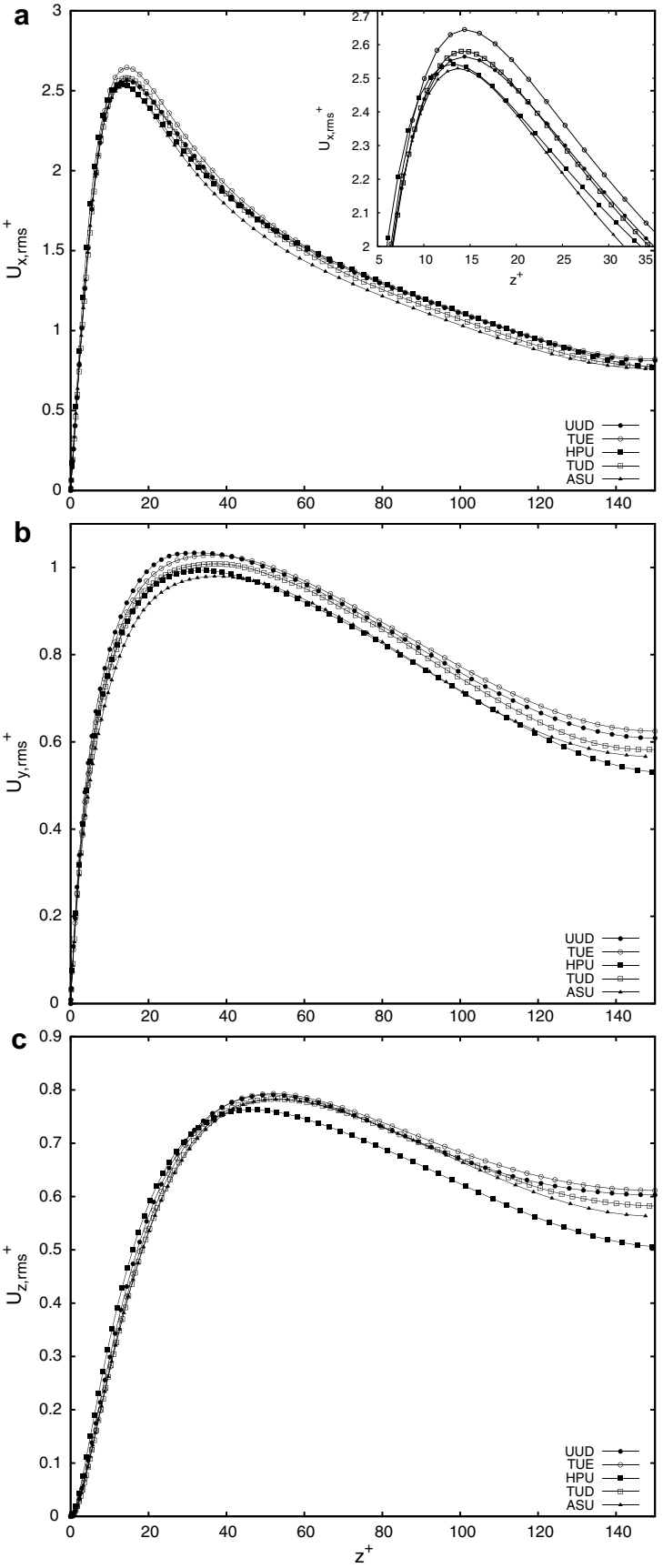

Fig. 3. Root mean square of fluid velocity fluctuations, $U'_{i,\mathrm{rms}}$.

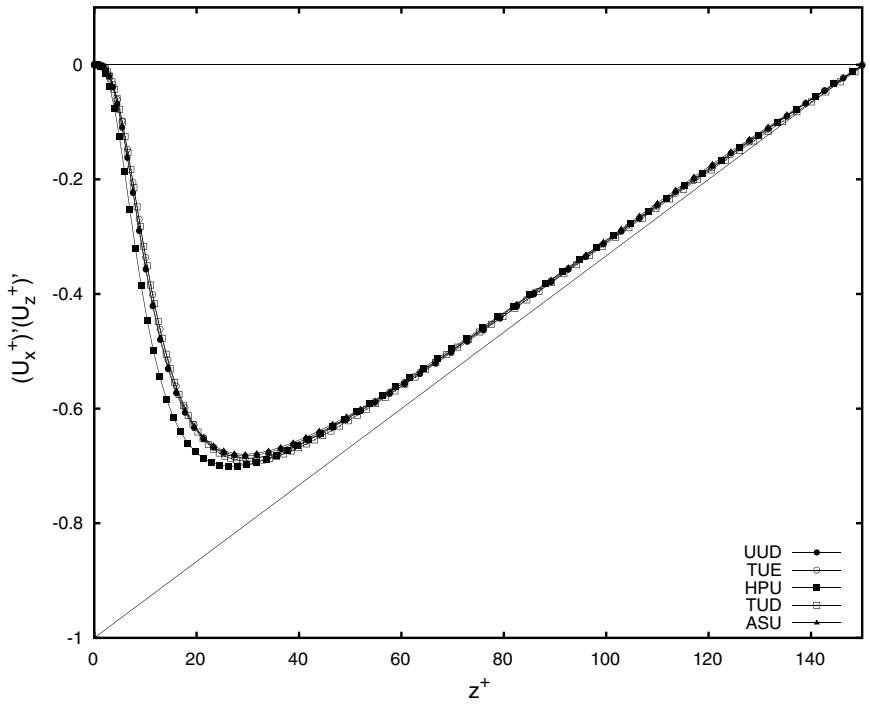

Fig. 4. Fluid Reynolds stress: $(U_x^+)'(U_z^+)'$ component.

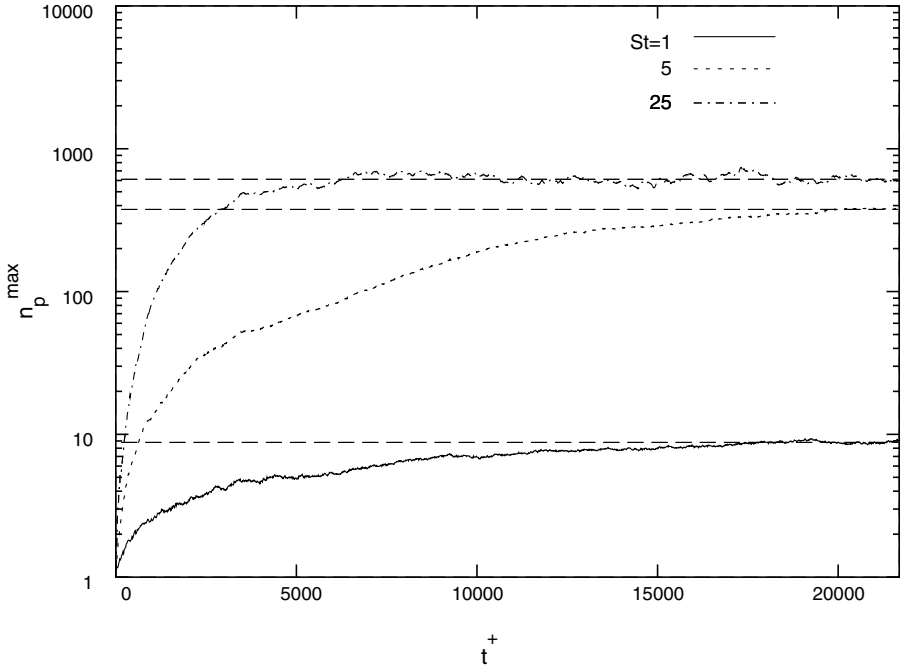

Fig. 5. Maximum value of particle number density at the wall, n_p^{max}, as function of time t^+ (lin–log plot). Data from Group UUD.

magnitude of this build up depends on the Stokes number of the particles. The steady-state concentration profiles, albeit being not physical (near-wall effects arise that are more complicated than those taken into account in the base simulation), are well consistent with all the information a DNS can provide. Also, the agreement between the profiles of each group increases with the particle Stokes number. For the two smaller particle sets ($St = 1$ and $St = 5$), quantitative differences in the predicted near-wall peak values are observed among all groups; however, the results of Group TUE match closely with those of Group TUD and there is a good agreement between the results of Group UUD and those of Group HPU (even if the shape of the profiles and the location of the peak value is different). Differences are still present for the higher inertia particles ($St = 25$), yet they become less evident in proportion. Unfortunately, for the $St = 1$ particles, it was not possible to include data from Group ASU due to their unavailability. Discrepancies in the quantification of local particle concentration arise not only because of the diverse numerical schemes and grid

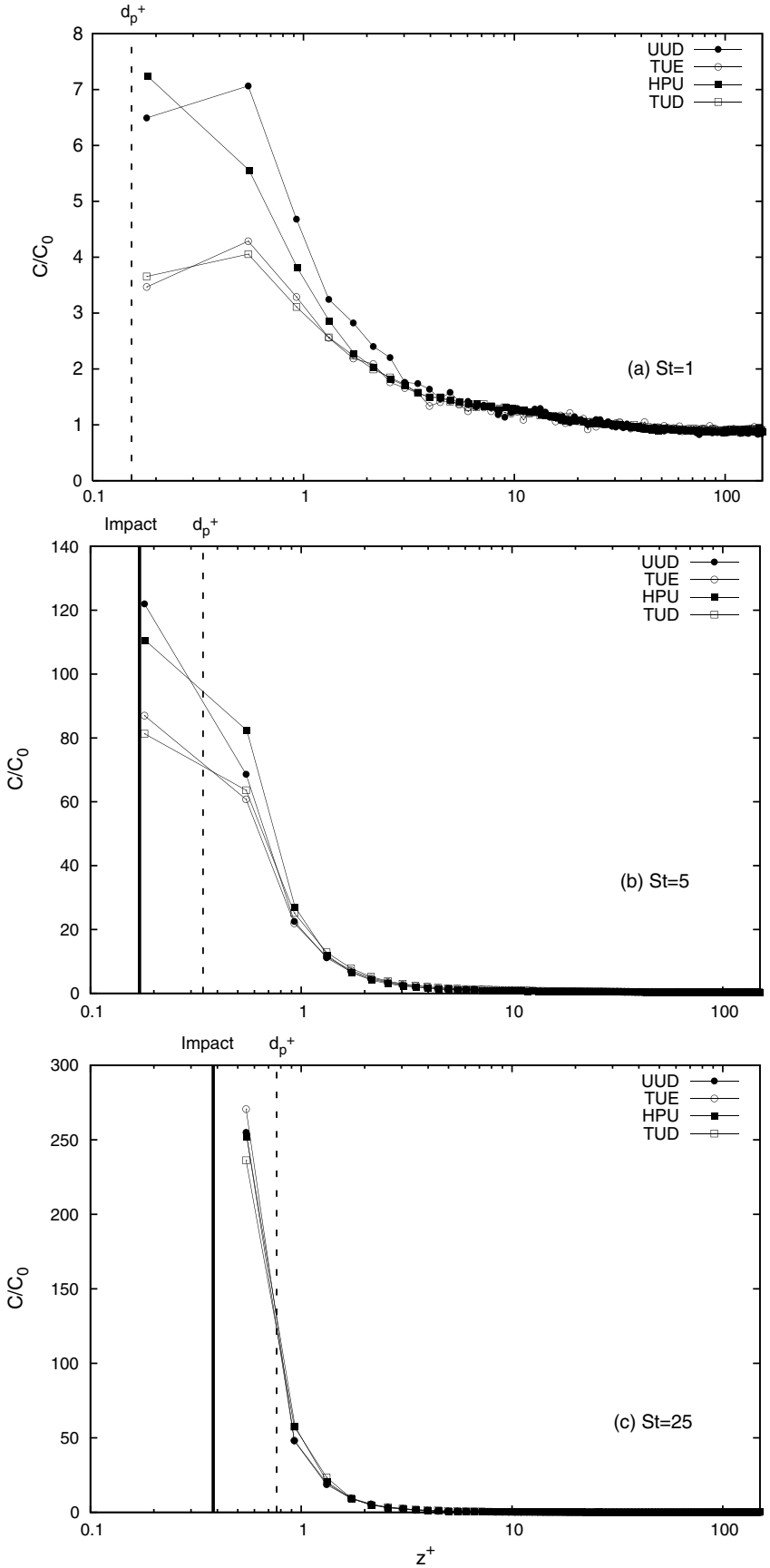

Fig. 6. Instantaneous particle number density wall-normal profiles, C/C_0 (log–log plot): (a) $St = 1$, (b) $St = 5$, (c) $St = 25$. The vertical solid line in each diagram indicates the position where the particles hit the wall (*Impact*); the vertical dash-dotted line gives a visual indication of the size of the particle diameter in wall units (d_p^+).

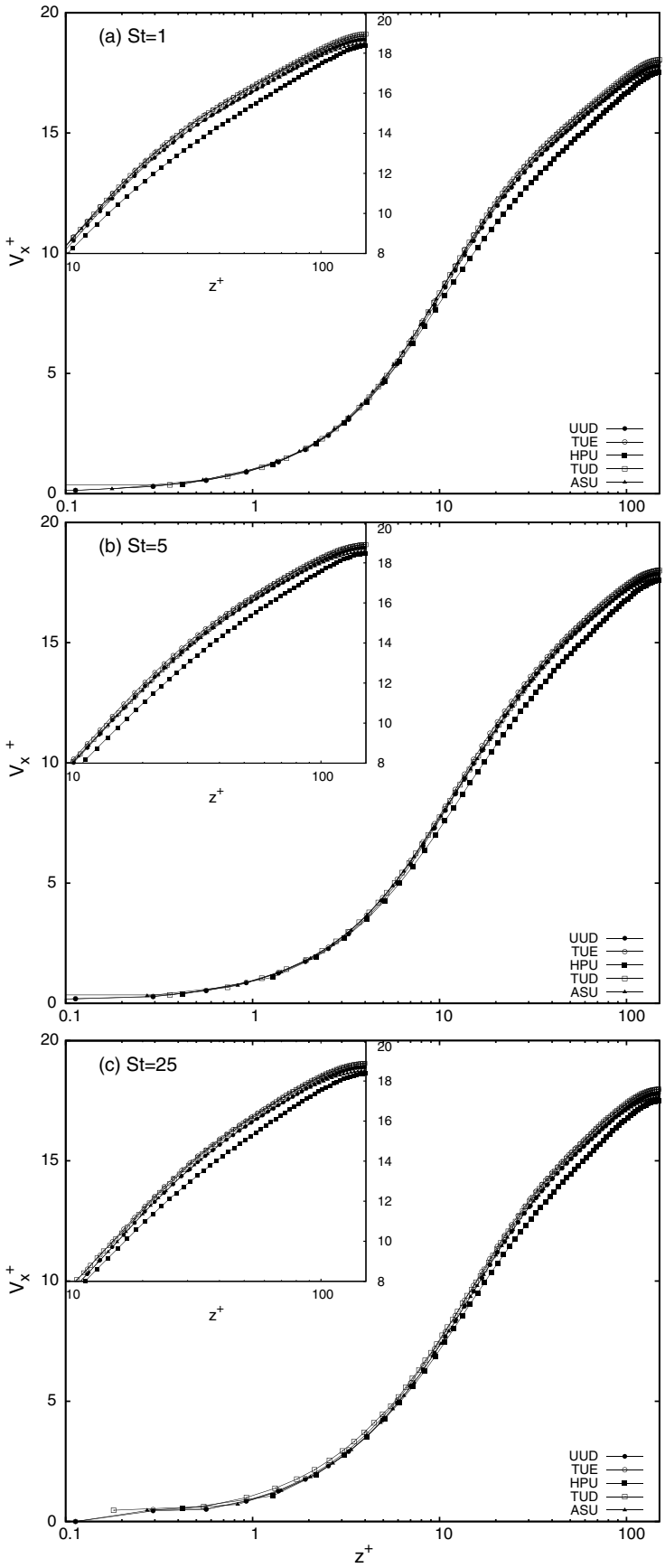

Fig. 7. Mean streamwise particle velocity, V_x^+. (a) $St = 1$, (b) $St = 5$, (c) $St = 25$.

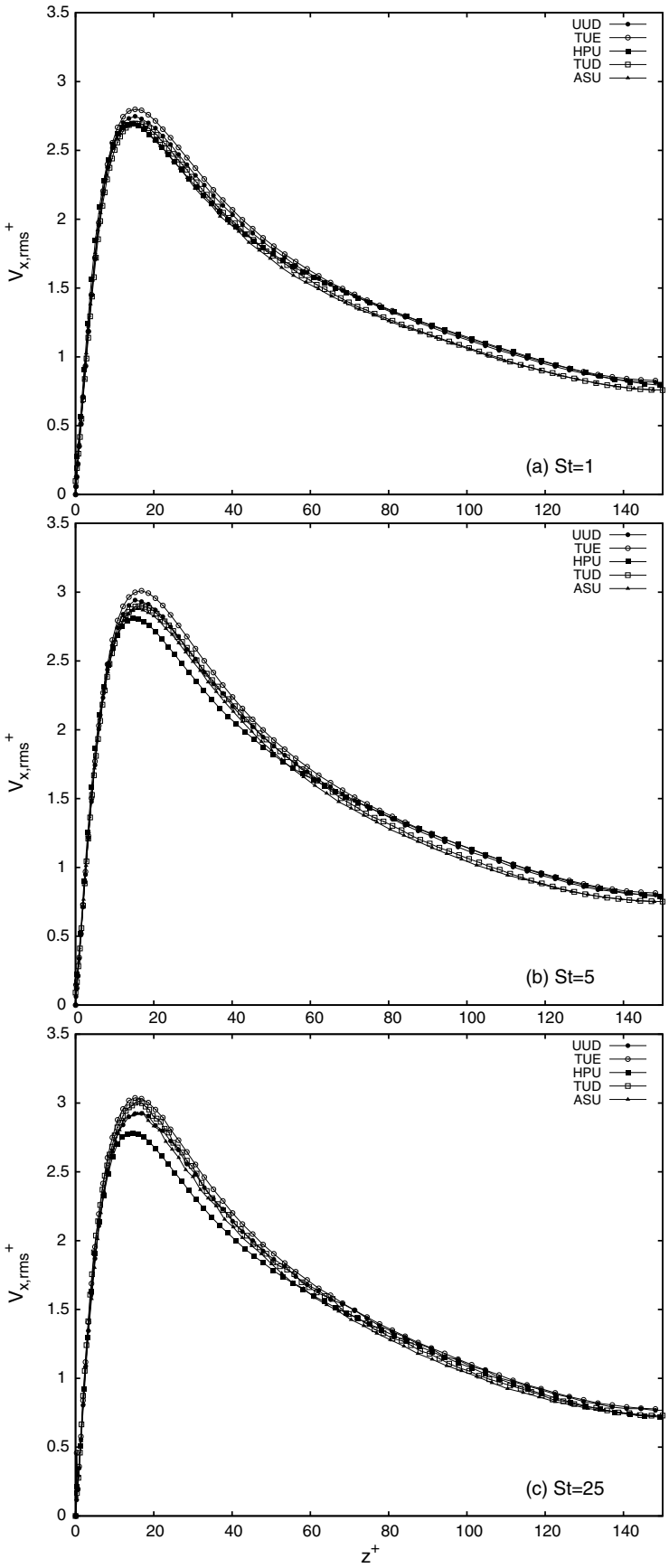

Fig. 8. Root mean square of particle streamwise velocity fluctuations, $V_{x,rms}^+$. (a) $St = 1$, (b) $St = 5$, (c) $St = 25$.

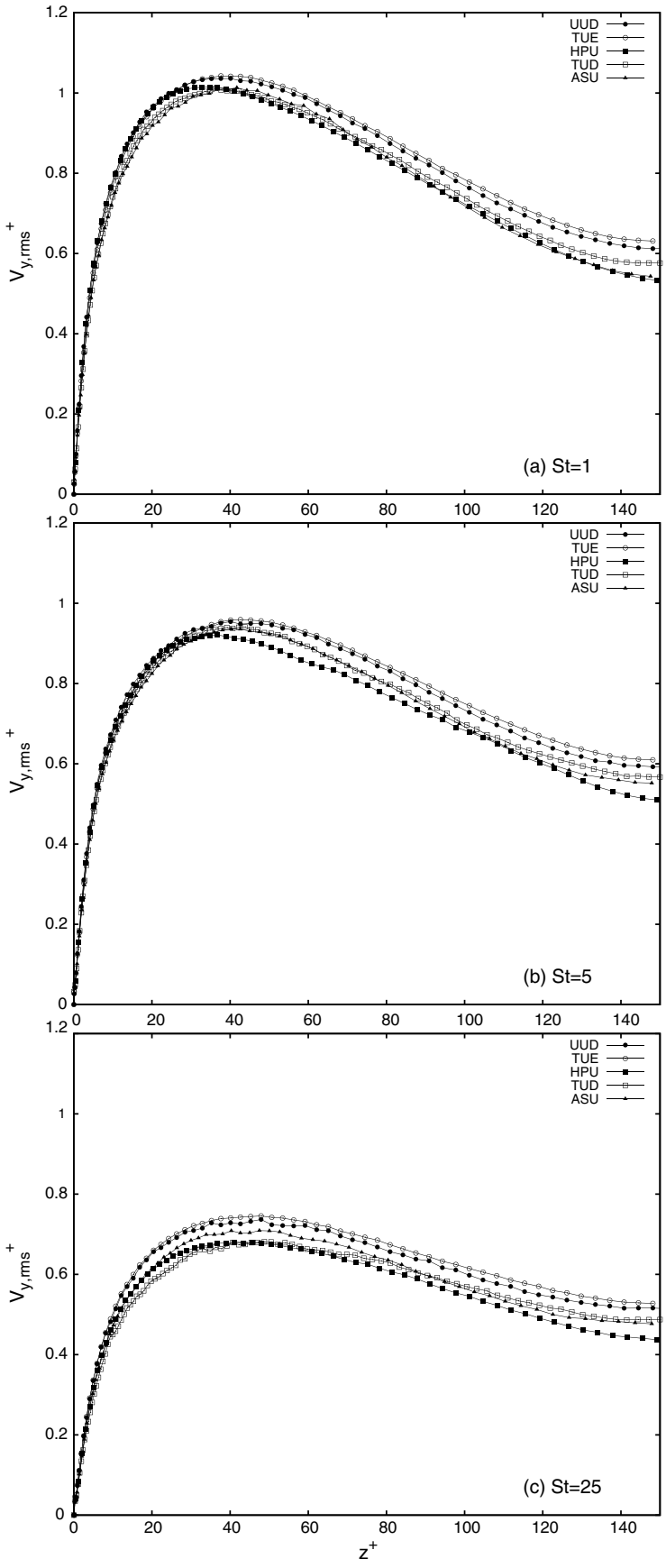

Fig. 9. Root mean square of particle spanwise velocity fluctuations, $V_{y,rms}^+$. (a) $St = 1$, (b) $St = 5$, (c) $St = 25$.

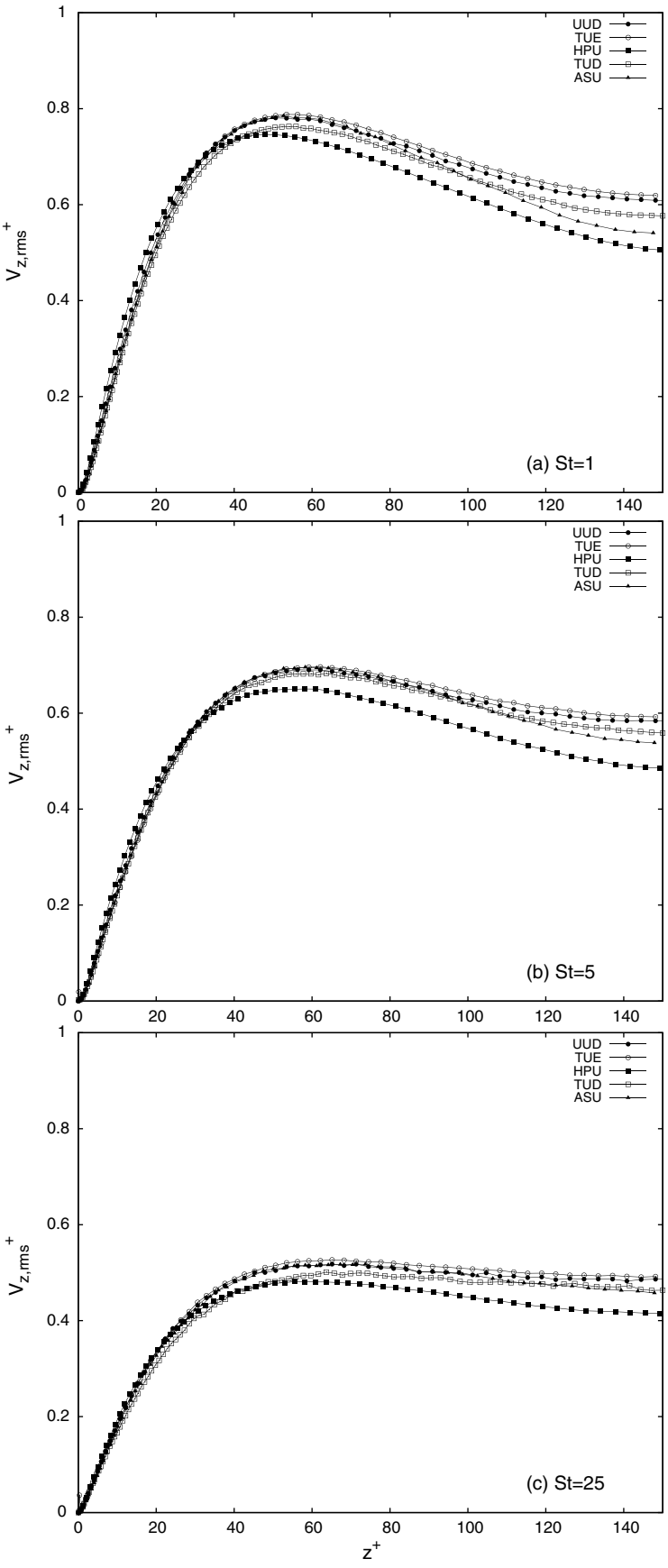

Fig. 10. Root mean square of particle wall-normal velocity fluctuations, $V_{z,rms}^+$. (a) $St = 1$, (b) $St = 5$, (c) $St = 25$.

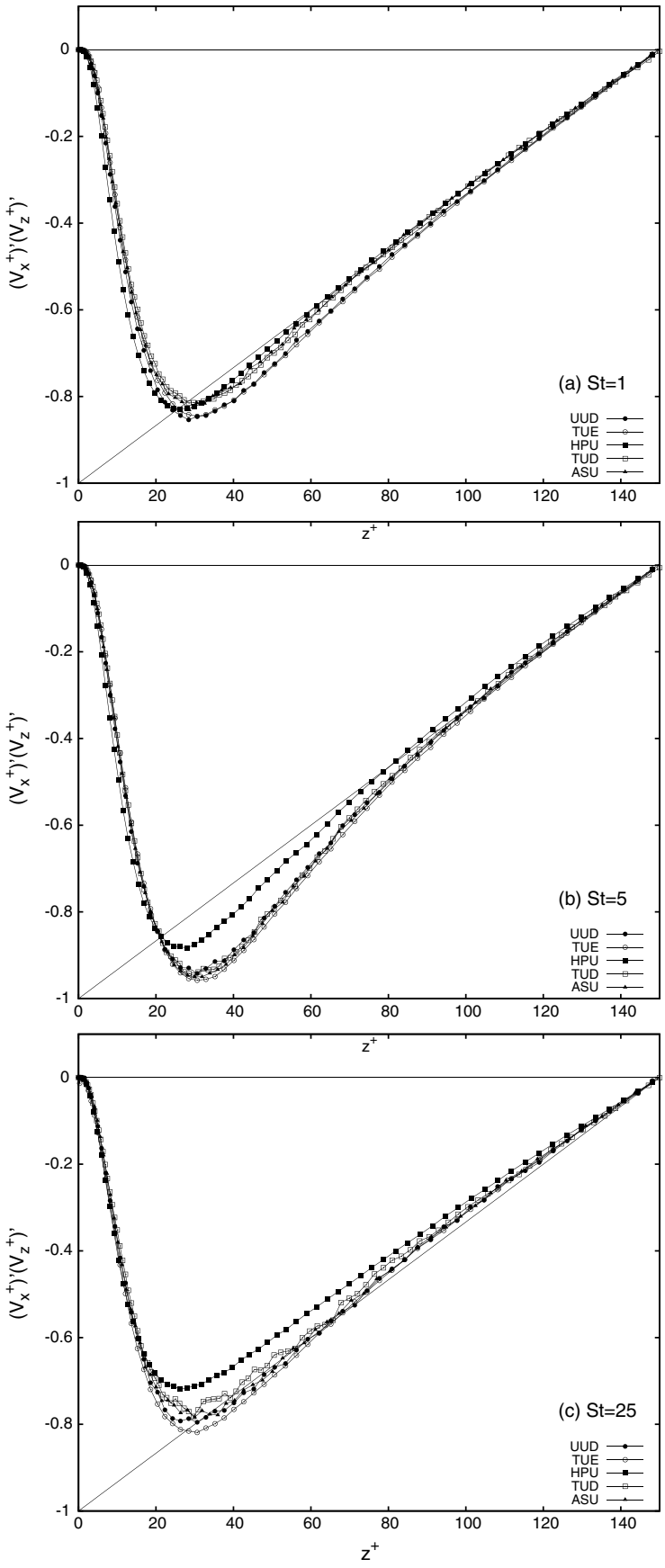

Fig. 11. Particle Reynolds stresses: $(V_x^+)'(V_z^+)'$ component. (a) $St = 1$, (b) $St = 5$, (c) $St = 25$.

discretizations adopted by each group but also, if not mainly, because of the numerical errors associated (i) with the different interpolation techniques used to obtain the fluid velocity at particle position and (ii) with the choice of the time-step size used to integrate the equation of motion for the particles. These numerical errors sum up over time and give the accumulated profile deviations observed in Fig. 6. It should be noted, however, that concentration profiles start to deviate significantly from each other only very close to the wall (roughly within one wall unit from the wall, a thickness that could be considered negligible from a pragmatic engineering perspective) and that deviations are magnified by the log–lin scale chosen to visualize the profiles. Also, we remark that the presence of discrepancies does not imply that only one of the profiles shown is correct while the others are wrong; rather, it implies that there might be a *best* prediction for a given statistical quantity which, however, is not known a priori. In other words, with the current data available it is not possible to conclude which is, if any, the best dataset. However, we can observe that the range of wall concentration predictions can be accepted as a good measure of particle wall concentration under the modelling assumptions used in this work.

The influence of making different choices in modeling the two phases is also apparent from particle velocity statistics. In Fig. 7, the mean streamwise velocity profiles, V_x^+, for the $St = 1$ particles (Fig. 7a), for the $St = 5$ particles (Fig. 7b) and for $St = 25$ particles (Fig. 7c) are shown. A close-up view has been included in the diagrams to highlight the behavior of V_x^+ in the outer layer of the channel. As observed for the fluid velocity, the agreement among mean quantities is quite satisfactory except for a velocity deficit in the log–law region. The profiles of the mean wall-normal velocity are not shown as they are equal to zero at steady state. In the database, however, the cross-stream profiles for the mean relative wall-normal velocity are provided. This velocity, computed as particle velocity minus fluid velocity *seen* by the particles, can be used to quantify the drift of particles to the wall when the simulation is not yet fully settled.

The rms of the particle velocity, $V_{i,rms}^+$, in the streamwise, spanwise and wall-normal direction are shown in Figs. 8, 9 and 10, respectively. From Fig. 8, it is apparent that the behavior of $V_{x,rms}^+$ near the centerline is well predicted by all groups, regardless of the Stokes number. Near the wall, however, the uncertainty associated with the calculation of the peak value is higher (even though the peak location is rather well predicted) and increases with St. In the spanwise (Fig. 9) and in the wall-normal direction (Fig. 10), the best agreement between the different groups is found in the near-wall region, whereas the rms profiles start to deviate from each other as we move towards the core region of the flow outside the buffer layer.

Analysis of the mean and rms values of particle velocity seems to indicate that single-point particle velocity statistics are not much affected by the different predictions of particle concentration. To corroborate this conclusion, in Fig. 11 we show the $(V_x^+)'(V_z^+)'$ component of the Reynolds stress tensor for the particles. Detailed knowledge of the elements of this tensor is crucial to validate theoretical models of particle deposition in wall-bounded turbulent flows that try to reproduce the convective wallward drift of particles by assuming local equilibrium between the particles and the fluid turbulence (see the deposition model by Young and Leeming (1997), for instance). The trend we can observe from Fig. 11 is similar to that observed for the rms of the particle velocities: there is a good agreement for the smaller particles and an increasing uncertainty associated with the calculation of the peak value for the larger particles. In particular, the profile of Group HPU is characterized by a smaller absolute value of the peak for both the $St = 5$ and the $St = 25$ particles which is likely related to an underprediction of the particle velocity fluctuations in the near-wall region as compared with the other groups. In Fig. 11 (and in Figs. 8–10 as well), some profiles appear to be a little bit ragged due to smaller intervals chosen for time averaging. The length of the averaging interval was one of the parameters that could be chosen by the participants. Here, a longer time span would have certainly smoothed out the profiles but it would have not changed their relative position within the chart.

One interesting aspect of the test case is that it gives the chance to single out the effect of each possible source of error on the observed results through a well-aimed parametric study. This study is not currently available (as it is beyond the scope of the benchmark calculation) but can be definitely regarded as a possible extension to the base simulation.

4. Conclusions

The dispersion of particles with finite inertia in wall-bounded turbulent flows is of fundamental importance for numerous applications in industry and environment. The dispersion process, however, is characterized by complex phenomena such as non-homogeneous distribution, large-scale clustering and preferential concentration in the near-wall region due to the inertial bias between the denser particles and the lighter surrounding fluid (Marchioli and Soldati, 2002; Eaton and Fessler, 1994). Direct Numerical Simulation, even at moderate Reynolds number, coupled with Lagrangian particle tracking has been widely used to study these macroscopic phenomena, for instance in vertical turbulent pipe (Vreman, 2007; Uijttewaal and Oliemans, 1996) and channel flows (Li et al., 2001; McLaughlin, 1989), and represents a useful tool to provide physical insights, new modeling ideas and benchmark cases (Moin and Mahesh, 2002; Yeung, 2002).

In this paper, we have presented the main results produced by an international collaborative test case in which direct comparison is made among the numerical predictions obtained by different computational codes for the common problem of turbulent particle dispersion in channel flow. A comprehensive database of statistics for the fluid and for the particles has been gathered and made available in the form of post-processed ASCII files at HTTP://CFD.CINECA.IT/CFD/REPOSITORY/. In addition to repository files containing the statistical datasets, the database includes raw data for the instantaneous fully developed flow field and for the particle position/velocity: these data are made available in the form of formatted ASCII files to users who need to compute specific statistics not yet included in the database. Another original (and very important) feature of the database is that it was collected under statistically steady condition for the particle distribution: the database may thus bring significant advantages both from the computational viewpoint (starting a new simulation with steady-state initial condition for the dispersed phase may allow large savings in terms of CPU time) and from the modeling viewpoint (the datasets may be used to validate closure approximations for models based on the assumption that the flow of the particle phase is fully developed: see Sergeev et al. (2002), for instance).

On the basis of the results discussed in this paper, the conclusions listed below can be drawn.

- The database represents a homogeneous source of data on DNS and LPT not previously available that can be used as a benchmark to test the performance of new numerical methods or as a tool to validate theoretical models for the gas–solid interactions in channel flow (for instance, models including a posteriori large-eddy simulations).
- Direct comparison of the statistics allows clearcut observation of (i) how different codes perform when applied to the same problem with a well-defined simulation setting and of (ii) how the

accuracy of the results depends on the choices made in terms of simulation parameter values. As demonstrated by the several previous papers published independently by each of the participating groups (see Marchioli and Soldati, 2002; Portela and Oliemans, 2003; Kuerten, 2006; Arcen et al., 2006 for instance) all methods have been used to produce DNS-quality data to investigate on the physics of turbulent particle dispersion in wall-bounded flows and/or to benchmark simpler models. However, direct comparison of the results brings to the following *caveat*: even when the most accurate numerical tools are used and all the simulation requirements are fulfilled, one may find non-negligible quantitative differences in the statistics. Of course, there will be a *best* prediction for a given statistical quantity, yet such best prediction is not known a priori. For this reason, it appears very difficult to provide clearcut indications on the reliability of each dataset: we can just observe that the range of wall concentration predictions can be accepted as a good measure of particle wall concentration under the modelling assumptions used in this work.

- Parametric studies performed apart from the base simulations are required to single out the effect of changing one simulation parameter (or more) from the macroscopic particle behavior.

The test case calculations can be regarded as a challenge to approach more complex problems in two-phase flow predictions and will hopefully stimulate further improvement and development of numerical methods and models. To this aim, test case calculations will be continued by extending the base simulation presented here. Specifically, all participant groups will include one or more additional simulation parameters. To compare results more easily, the choice will be restricted to parameters dealing with the physical modeling of the flow, such as fluid–particle two-way coupling, inter-particle collisions, lift force models and sub-grid scale effects on particle motion in large-Eddy simulation fields. Further parameter analysis will be planned at a later stage and other statistical quantities will be made available as they are extracted from the simulations.

Acknowledgement

We thank the Cineca supercomputing center (Bologna, Italy) for the hosting of the DNS database.

References

Arcen, B., Tanière, A., Oesterlé, B., 2006. On the influence of near wall forces in particle-laden channel flows. Int. J. Multiphase Flow 32, 1326–1339.

Balachandar, S., Prosperetti, A. (Eds.), 2006. IUTAM Symposium on Computational Approaches to Multiphase Flow: Proceedings of an IUTAM Symposium held at Argonne National Laboratory, October 4–7, 2004. Springer, Dordrecht, The Netherlands.

Eaton, J.K., Fessler, J.R., 1994. Preferential concentration of particles by turbulence. Int. J. Multiphase Flow 20, 169–209.

Elghobashi, S., Truesdell, G.C., 1992. Direct simulation of particle dispersion in a decaying isotropic turbulence. J. Fluid Mech. 242, 655–700.

Goldensoph, G.M., 2006. The influence of filtering on the motion of heavy particles in gas-phase turbulence. M.S. Thesis, Department of Mechanical and Aerospace Engineering, Arizona State University, 2006.

Kuerten, J.G.M., 2006. Subgrid modeling in particle-laden channel flow. Phys. Fluids 18, 025108.

Li, Y., McLaughlin, J.B., Kontomaris, K., Portela, L., 2001. Numerical simulation of particle-laden turbulent channel flow. Phys. Fluids 13, 2957–2967.

Marchioli, C., Soldati, A., 2002. Mechanisms for particle transfer and segregation in turbulent boundary layer. J. Fluid Mech. 468, 283–315.

Marchioli, C., Picciotto, M., Soldati, A., 2006. Particle dispersion and wall-dependent fluid scales in turbulent bounded flow: implications for local equilibrium models. J. Turbulence 7, 1–12.

McLaughlin, J.B., 1989. Aerosol particle deposition in numerically simulated channel flow. Phys. Fluids 1, 1211–1224.

Moin, P., Mahesh, K., 2002. Direct numerical simulation: a tool in turbulence research. Ann. Rev. Fluid Mech. 30, 539–578.

Orlandi, P., 2000. Fluid Flow Phenomena – A Numerical Toolkit. Kluwer Academic Publishers, London.

Portela, L.M., Oliemans, R.V.A., 2003. Eulerian/Lagrangian DNS/LES of particle–turbulence interactions in wall-bounded flows. Int. J. Numer. Meth. Fluids 43, 1045–1065.

Rowe, P.N., Enwood, G.A., 1962. Drag forces in hydraulic model of a fluidized bed – Part I. Trans. Inst. Chem. Eng. 39, 43–47.

Sergeev, Y.A., Johnson, R.S., Swailes, D.C., 2002. Dilute suspension of high inertia particles in the turbulent flow near the wall. Phys. Fluids 14, 1042–1055.

Sommerfeld, M. (Ed.), 2005. Proceedings of the 11th Workshop on Two-Phase Flow Predictions, CD-ROM.

Uijttewaal, W.S.J., Oliemans, R.V.A., 1996. Particle dispersion and deposition in direct numerical and large eddy simulations of vertical pipe flows. Phys. Fluids 8, 2590–2604.

Tian, L., Ahmadi, G., 2007. Particle deposition in turbulent duct flows – comparisons of different model predictions. J. Aerosol Sci. 38, 377–397.

Vreman, A.W., 2007. Turbulence characteristics of particle-laden pipe flow. J. Fluid Mech. 584, 235–279.

Yeung, P.K., 2002. Lagrangian investigation of turbulence. Ann. Rev. Fluid Mech. 34, 115–142.

Young, J., Leeming, A., 1997. A theory of particle deposition in turbulent channel flow. J. Fluid Mech. 340, 129–159.